 doi:10.20944/preprints202012.0011.v1

Article

Forced fold amplitude and sill thickness constrained by wireline and 3-D seismic data suggest an elastic magma-induced deformation in Tarim Basin, NW China

Wei Tian*, Xiaomin Li, Lei Wang

School of Earth and Space Sciences, Peking University, Beijing 100871, China

* Correspondence to: Wei Tian at davidtian@pku.edu.cn

Abstract: Disparities between fold amplitude (A) and intrusion thickness (H_{sill}) are critical in identifying elastic or inelastic deformation in a forced fold. However, accurate measurement of these two parameters is challenging because of the limit in separability and detectability for the seismic data. In the TZ-47 exploring area from the Tarim Basin, Northwest China, we combined wireline data and 3-D seismic data, to accurately constrain the fold amplitude and total thickness of sills that inducing the roof uplift. The measurement results show that the forced fold amplitude is 155 m and the total sill thickness is 148.4 m. When using a magma density of 2.7 g/cm^3, and solid rock density of 3 g/cm^3, the molten magma thickness at the time of intrusion would be 153.8 m, which is almost no difference from the forced fold amplitude. Therefore, the TZ-47 fold is a pure elastic forced fold induced by emplacement of multiple sills. Measurement solely based on seismic data may not be able to detect some thin interlayers and may result in large errors.

Keywords: forced fold; elastic; inelastic; saucer-shaped sill; wireline data; seismic cube; velocity pull up; Tarim flood basalt

1. Introduction

Shallow-level sills and laccoliths are commonly accommodated by bending and uplift of the overlying rock and free surface [1-6]. The morphology of this "roof uplift" is considered to mimic the geometry of underlying intrusion(s) and is thus described as a form of "forced fold" [7]. Based on an elastic model, Pollard and Johnson [6] proposed that amplitude of forced folds has a simple relationship with the morphology of subsurface magma: when the intrusion diameter (D) to emplacement depth (d) ratio is >>4, the original intrusion thickness (H_{sill}) broadly equals the original amplitude (A) of the overlying forced fold (i.e., $A/H_{sill} = 1$). Therefore, measurement of ground deformation has been widely used in determining the shape of subsurface magma and forecasting volcanic hazard [8-11] .

However, recent field, modeling and seismic interpretation studies have questioned the elastic model based on that the forced fold amplitude is less than the thickness of subsurface magma in different extent [12]. In addition to elastic uplift, inelastic space-making process can also accommodate intrusive magma, meaning that the extent of surface uplift may not equal to that of the underlying magma reservoir [13-18].

 doi:10.20944/preprints202012.0011.v1

Therefore, accurate measurement of the disparity between intrusion thickness and forced fold amplitude has become a major challenge in identifying elastic and inelastic deformation in seismically imaged sill-fold pairs [3,19-21]. In practice, direct measuring of sill thickness in active volcanic systems is impossible, and so does with seismic data alone because inversion of seismic thickness to true thickness brings significant uncertainty and, in some instance, relies on human perception. Lack of precise thickness data of the overburden host rocks in seismic analysis also limits accurate estimation of the forced fold amplitude.

In this contribution, we report a combined seismic (i.e., interpreted thickness) and wireline (i.e., true thickness) dataset beneath a magma intrusion-induced forced fold from Central Tarim Basin, NW China. Based on the comparison of the "true forced fold amplitude" (A) and the "true sill thickness" (H_{sill}), we show that elastic component is dominant in the deformation of a subsurface volcano system.

2. Geological setting and data cube descriptions

The Tarim Basin is an endorheic basin occupying an area of over 600,000 km^2 in northwest China. It is bounded by the Tianshan Mountains to the north and northwest, the Altyn Mountains to the southeast and the Kunlun Mountains to the southwest (Fig. 1). The Taklamakan Desert dominates the surface of the Tarim Basin. A thick succession of Phanerozoic strata, which covers the central parts of the basin, locally exceeds 10 km in thickness [22]. The basement of the basin is a Precambrian block that is considered to be a fragment of the Rodina Supercontinent [23,24]. The Cambrian System consists of a succession of gray to dark gray limestone and dolomite with salt layers, which were deposited in an evaporative/carbonate platform environment [22]. The Ordovician carbonate system is predominantly composed of thick limestone and dolomites associated with an open platform. The Silurian and Devonian sedimentary succession primarily comprises sandstones and mudstones deposited in a tidal-flat environment. The Carboniferous System consists of sandstone and limestone with intercalated mudstone formed in marine-terrigenous facies. Strata in the Permian System are mainly sandstone, mudstone and volcanic lava flows in a terrigenous environment. Major unconformities occur at the Middle - Upper Ordovician boundary, the Silurian - Ordovician boundary and the Permian - Triassic boundary.

Preprints (www.preprints.org) | NOT PEER-REVIEWED | Posted: 1 December 2020 doi:10.20944/preprints202012.0011.v1

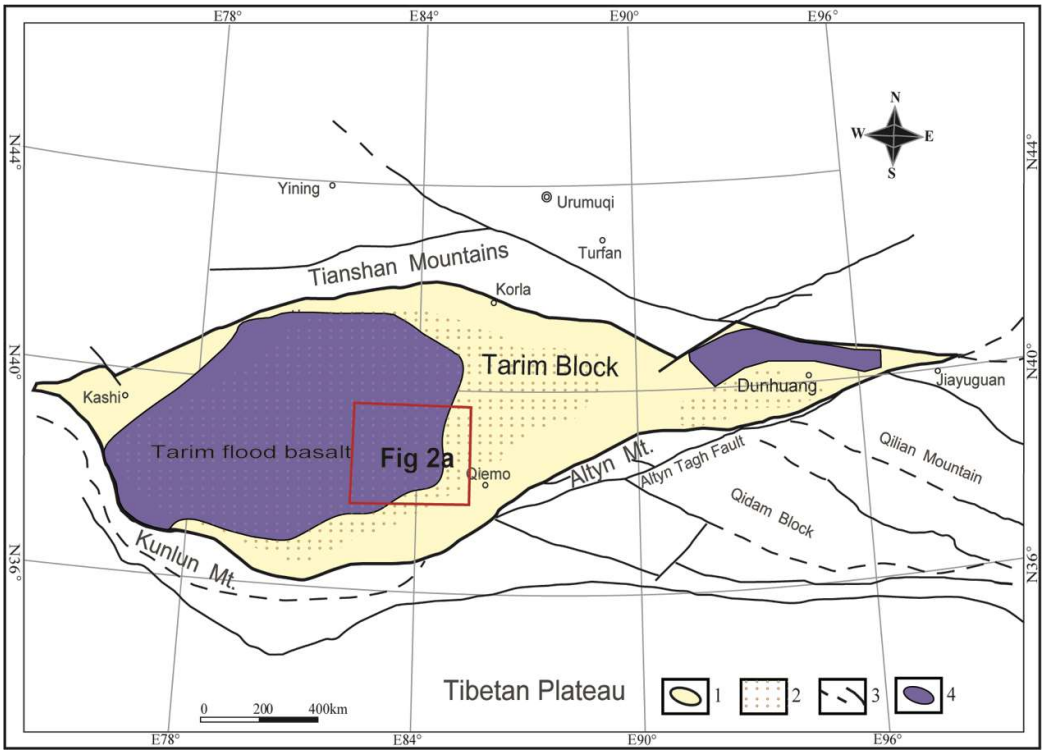

Fig. 1 Sketch geological map showing the spatial distribution of the early Permian Tarim flood basalt. Study area is shown in the map. Legend: 1, the Tarim Block; 2, desert; 3, major faults; 4, estimated distribution of the Tarim flood basalt.

The early Permian flood basalt composes the most voluminous volcanic successions in Tarim basin. At outcrop, the basalts occur in the Kupukuziman Formation and the Kaipazileike Formation [22]. The thickness of exposed basalt lava flows is up to 780 m [25], and the maximum thickness of the subsurface basalts exceeds 2500 m in Northern Tarim [26] and 1100 m in Central Tarim [27]. The total area of the subsurface lava flows estimated by petroleum industrial drilling, physical logging and seismologic reflection data is over 265,600 km^2 (Fig. 1). Olivine-tholeiitic basalt lava flows with OIB-like geochemistry erupted onto the upper Permian system at ~291-287 Ma [26,28]. The basalts were subsequently eroded, demarcated by an unconformity between Permian and Triassic strata.

The TZ-47 field hosts major petroleum and gas reservoirs in the Central Tarim Fields of PetroChina Co. Ltd. Several major faults, including the Tazhong-1 and Tazhong-2 faults were surveyed by 3-D industrial seismic interpretation (Fig. 2a). Wireline data from 21 wells in the area have revealed the presence of thick basalt lava flows at depths of 3300–3800 m across the whole area, as well as subvolcanic facies and volcanic vent facies sills at the depths of 3900–4500 m [27,29]. All the basalts are underlain by terrestrial sandstone, siltstone, or mudstone, implying subaerial eruptions. Industrial drilling and seismic interpretation have revealed several central volcanoes (Fig. 2b).

Preprints (www.preprints.org) | NOT PEER-REVIEWED | Posted: 1 December 2020 doi:10.20944/preprints202012.0011.v1

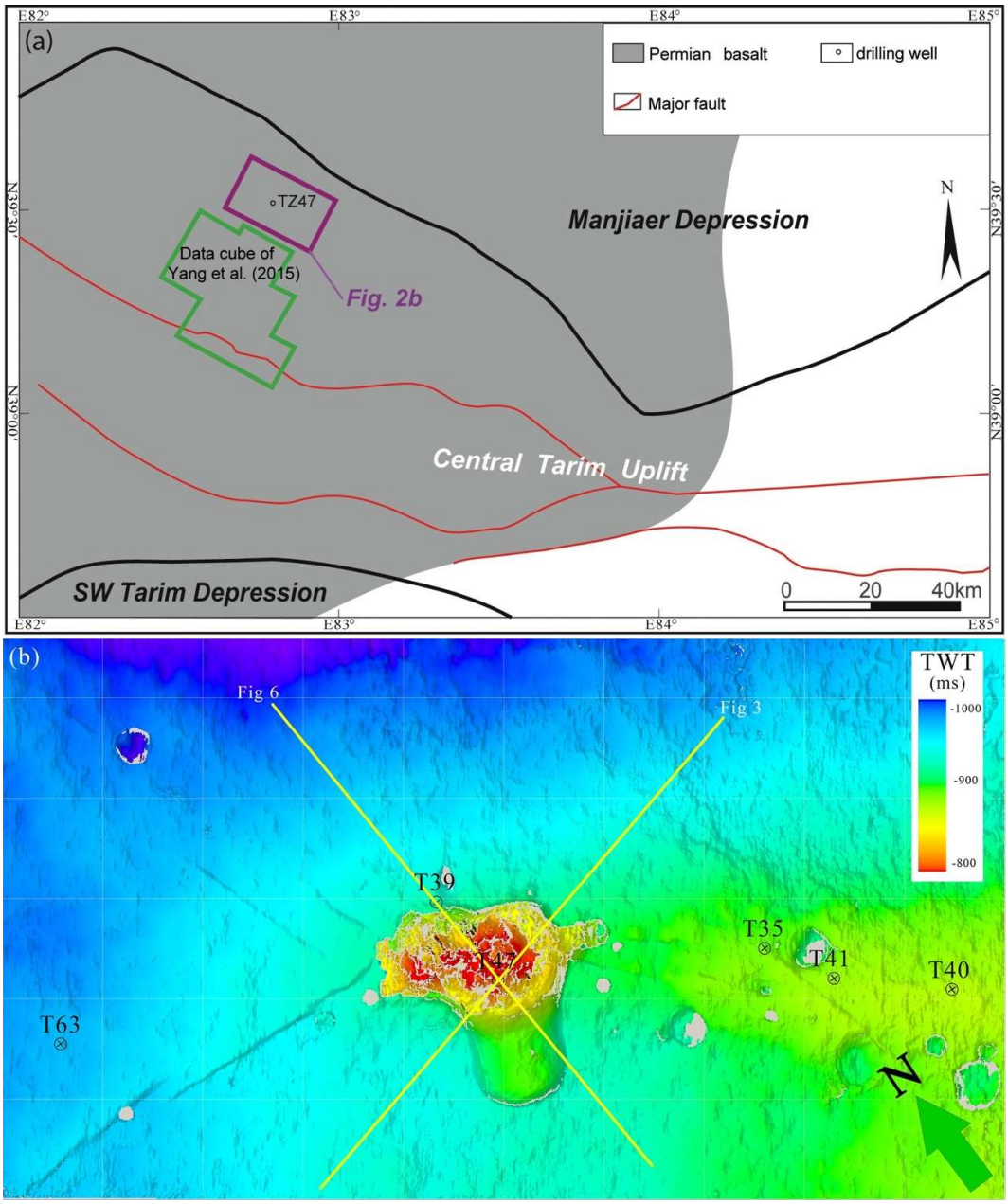

Fig. 2 Maps of the study area. (a) Sketch geological map of in the Central Tarim uplift showing the tectonic division, major faults and distribution of the Tarim flood basalt. Seismic cube in the study area is shown as purple rectangle in (a), which is to the northeast of the seismic cube studied in Yang et al. [27]; (b) Colour-visualized T0-isopleth showing the surface of the Permian basalt layer and the locations of the drilling wells in the study area. Thick yellow lines in (b) represent the location of two seismic profiles.

3. Data set and processing methods

The project database consists of a 3-D seismic cube covering approximately 600 km^2 in the TZ-47 field (Fig. 2a), which is to the north of the data cube of Yang et al. [27]. Six exploration drilling wells which intersect basaltic lava flows or subvolcanic intrusions are shown in Fig. 2b to confirm the

Preprints (www.preprints.org) | NOT PEER-REVIEWED | Posted: 1 December 2020 doi:10.20944/preprints202012.0011.v1

location of the igneous layers. Data acquisition of the seismic cubes was completed by the Tarim Oil Field Company (TOFC), PetroChina Co. Ltd, with 20 m line spacing and a positive reflection coefficient represented by positive amplitude and a black peak. Seismic data were processed by Bureau of Geophysical Prospecting (BGP) Inc., China National Petroleum Corporation. Interpretation was based on analysis of the pre-stack time-migrated (PSTM) data. Well log data were also supplied by TOFC. The physical logging data of drilling wells were tied to the seismic data by standard synthetic seismogram on the "Petrel E&P" Software Platform. Logging data of well TZ47 was tied to the seismic data for reads of accurate depths of the basalt and two sills; horizon picking is then conducted automatically from these reflectors (Fig. 3).

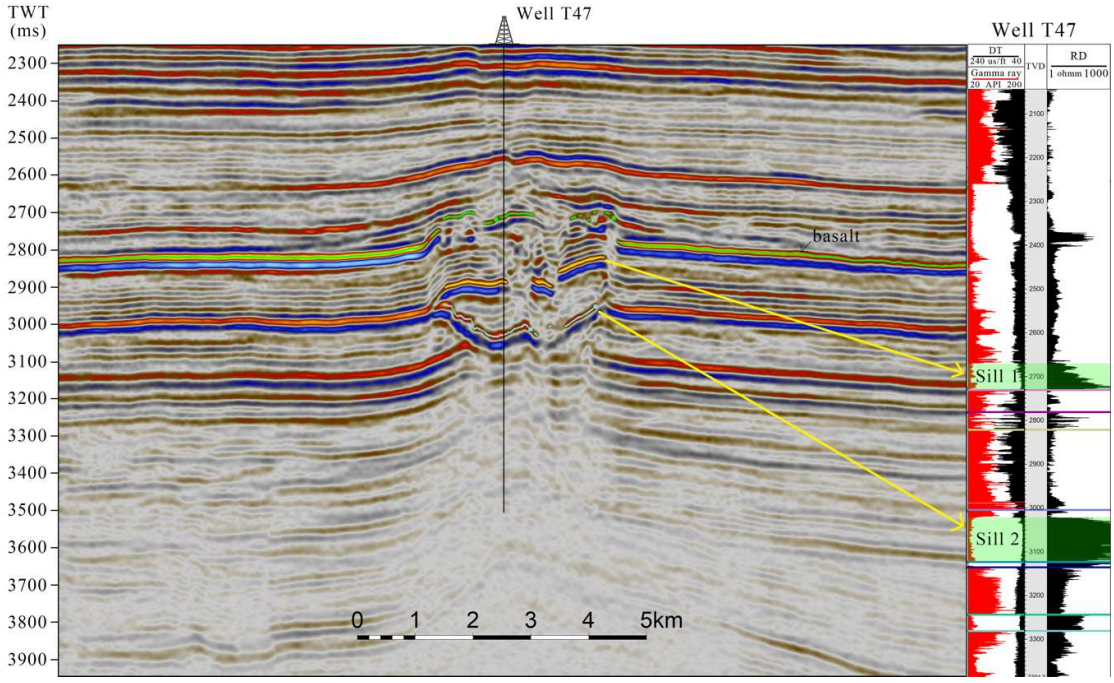

Fig 3. Seismic profile across well TZ47, illustrating the geometry, scale, and seismic expression of two basaltic sills in TZ47 area, and their correlations with down-well logging data.

Basaltic lava flows and sill-like intrusions are typically characterized by very high-amplitude reflections in seismic datasets, owing to the high energy-reflection at the contacts between the basalt and the clastic rocks [30]. Therefore, a lava flow can be easily isolated as a "geo-body" from surrounding clastic rocks in a 3D seismic dataset by using opacity rendering techniques, which can make the surrounding host-rock transparent [30-34]. In order to obtain the best resolving power, we pick out the 50~80 Hz high frequency components to interpret the basaltic rocks, which have an average velocity of 5500 m/s. The maximum resolving power or limit of separability of this method equals to $\lambda/8$ [11,12], which is 8.6 m (5500 m/s ÷ 80 Hz ÷8). Therefore, we can identify sills with thickness around 10 m.

During the seismic data processing, manual interpretation was combined with automated geo-body extraction, which allows us to study the morphology and geometry of subsurface igneous sill-dyke networks. The manual operation allows a better quality-control on the interpretation, particularly with the irregular distributed sill-dyke networks in clastic sedimentary rocks.

 doi:10.20944/preprints202012.0011.v1

In conjunction with the seismic study, an integrated study of the well data, including physical logs, geological reports and mud logs, was carried out in order to identify the sill complexes.

4. Results

4.1. Pre-deformation thickness of the host strata

A necessary prerequisite for accurate measuring of the forced fold amplitude is knowledge of the exact thickness of the host rocks. We use two horizon markers to examine the evenness of the sedimentary strata underlie the basalt layer. The upper marker is the top of the lower Permian basalt and the lower marker is the Upper Carboniferous "standard limestone", which is about 1000 m below the basalt layer and has a stable distribution across the Tarim Basin. In petroleum exploration practice, this limestone reflector is named "C4" for basin-wide seismic correlations. The thickness between these two markers is shown as a coloured contour map in Fig. 4a. It is noted that areas subject to influence of faulting and volcanic doming were excluded in thickness analysis and masked by pale grey colour.

In the thickness histogram (Fig. 4b), the thickness data have a mean value of 643.29 m with a standard deviation of 9.98 m. However, these data are bias from normal distribution because there is a locally high thickness (655~670 m) area in the lower right area, which is marked by a thick dashed red line (Fig. 4a). We compare the seismic reflectors of the basalt lava flow in this area with that from elsewhere and show the contrasting seismic characteristics in Fig. S1. The bottom reflector (blue one) of the basalt layer from the high thickness area are tuned, which means the thickness of basalt here has reached the tuning limit. Wells T40 and T41, which have basalt thickness of 72 m and 76 m, show tuning effect; while wells T39 and T35, which have basalt thickness of 52 m and 62m, show no tuning effect. This suggests that the tuning point should be slightly lower than 70 m, which is concordant with a tuning point at 25 Hz main frequency and a velocity of basalt at 5800 m/s. Therefore, we conclude the bias from normal distribution of the thickness data is caused by extra cumulation of lava flows in the lower right area, which has ~20m extra thickness according to the tuning effect of the basalt layer. When this area is excluded, the thickness becomes following normal distribution. The ~20m extra thickness of the lower right area can be easily explained by over-cumulation of lava flow at a down-slope area, which was resulted from the pre-eruption uplift of the Tarim flood basalt. The maximum vertical uplift before eruption of the Tarim flood basalt across a distance of 300 km has been estimated to be 887 m [35]. The dimension of the TZ-47 study area is 20-30 km, and the slope fluctuation can be ~60 – 90 m if the maximum vertical uplift is applied to this area, although the sloping in this local area seems to be less than one third of the maximum uplift sloping.

Preprints (www.preprints.org) | NOT PEER-REVIEWED | Posted: 1 December 2020 doi:10.20944/preprints202012.0011.v1

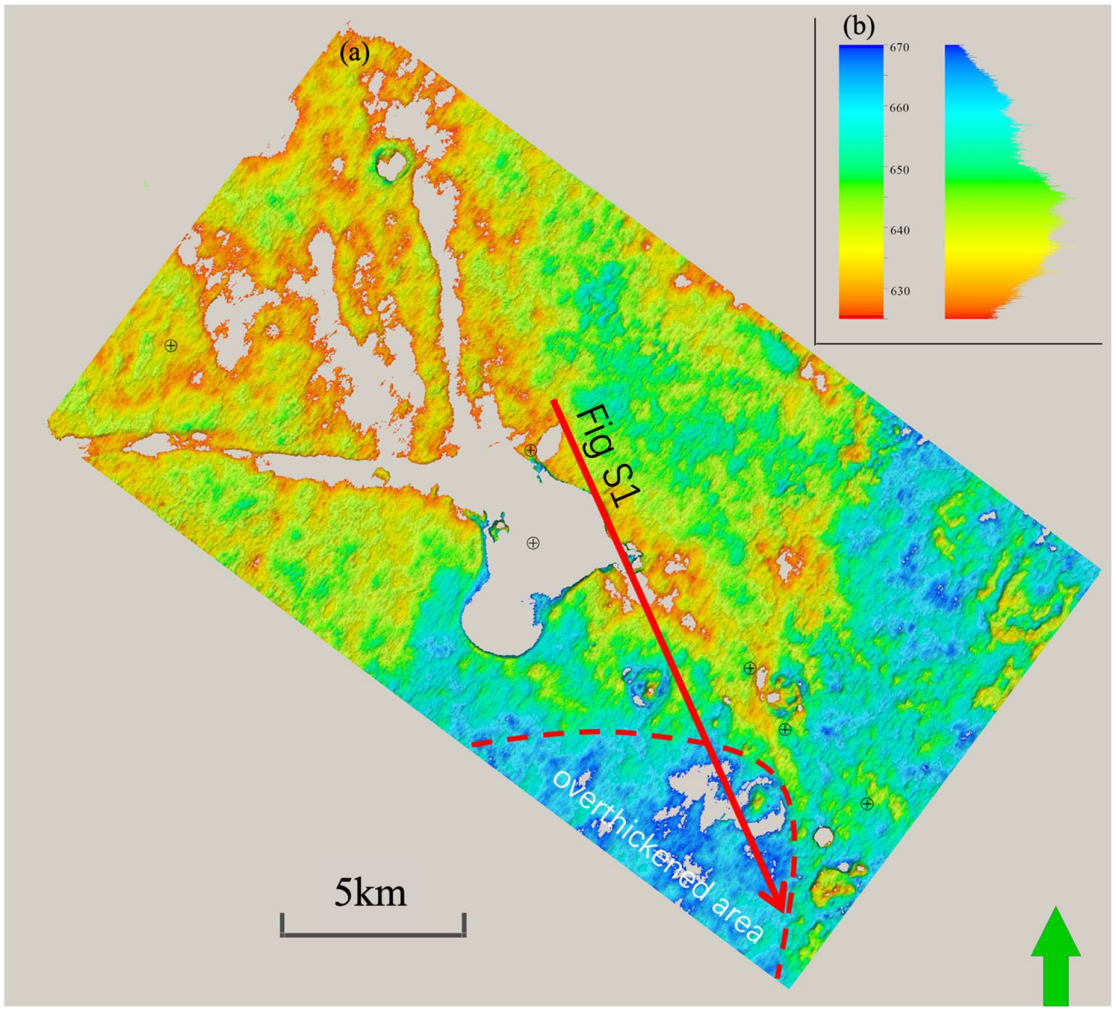

Fig. 4 Thickness of the sedimentary strata showing the evenness of the host rocks.

(a) Thickness isopleth of strata from the basalt top to the "standard limestone"(C4 reflector), grey color indicating eliminated areas subject to sill intrusion and faulting; (b) Statistics of the thickness data. The overall mean value of all thickness data is 643.29 m, with a standard deviation of 9.98 m, which is biased from normal distribution due to the existence of overthickened area as circled by dashed red line at lower right of (a). The red arrow indicates the strike of seismic profile Fig. S1.

4.2 Saucer-shaped sills measured by combination of wireline and seismic data

The “sill 2” intersected by drilling well T-47 at depth of 4100 m to 4200 m (Fig. 3) is a typical saucer-shaped sill complex. The geo-body corresponding to the top surface of this sill is shown in Fig. 5, which has a high amplitude reflection and is easily extracted from the seismic cube. Thickness of the inner sill of this saucer can be directly read from the stratigraphic column of T-47 (Fig. 6), which is 100.4 m. Chip and core identifications show that this sill is a typical dolerite. It can be identified in the well logging curves, which is characterized by low gamma value (GR<30 API) and high resistivity (RD>8 ohmm) (Fig. 6). The bottom of this sill is in contact with the “standard limestone”, which has velocity of 6000 m/s, similar to that of the sill (5800 m/s). This makes the sill bottom reflector cannot

Preprints (www.preprints.org) | NOT PEER-REVIEWED | Posted: 1 December 2020 doi:10.20944/preprints202012.0011.v1

be clearly identified. We therefore interpret the reflector of the "standard limestone" as the bottom limit of the "sill 2".

Reflector of "sill 1" is intercalated with several strong reflectors, and it is difficult to extract the geo-body of this sill complex. At the intersection with drilling well T-47, thickness of "sill 1" reads 62.5m.

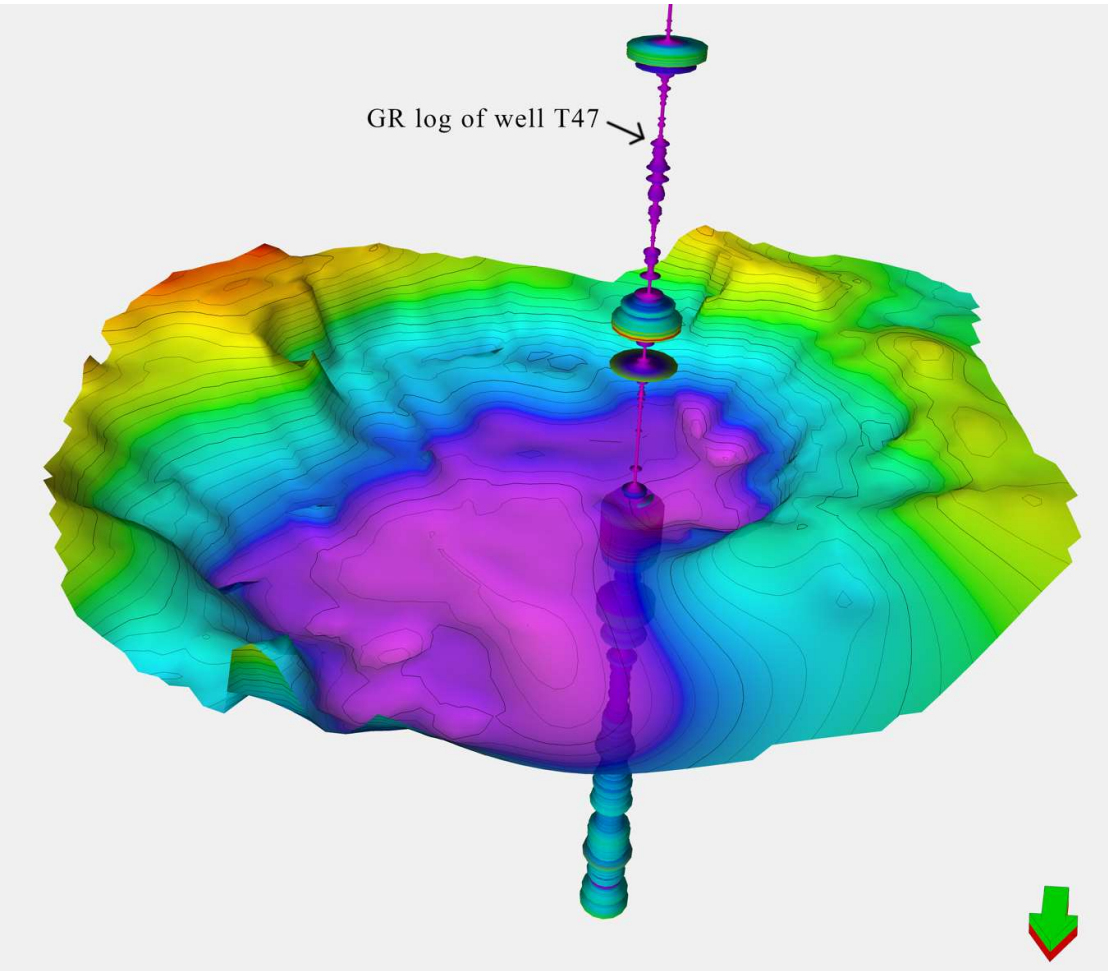

Fig. 5 Seismic geo-body of a saucer-shaped sill ("Sill 2" in Fig. 3) in three dimensions (3-D) and the location of drilling well T47 which intersected the saucer at depth of 4100 m-4200 m. The GR log is attached to drilling well T47.

Preprints (www.preprints.org) | NOT PEER-REVIEWED | Posted: 1 December 2020 doi:10.20944/preprints202012.0011.v1

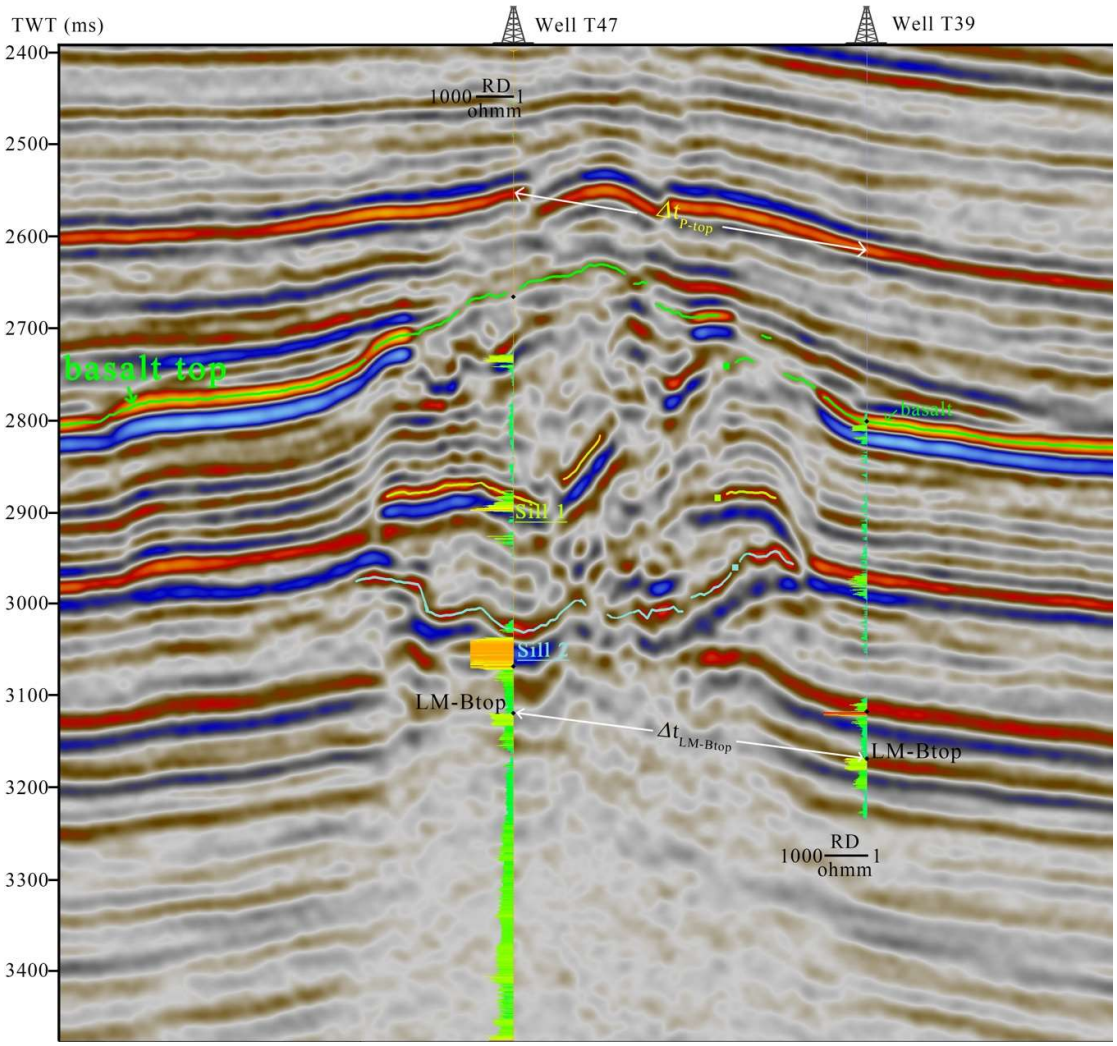

Fig 6. Seismic profile crossing well T47 and T39.

The bright green bars show the down-well log data of GR in time domain. The time structure difference of T39 and T47 at P-top is 58 ms, while that at the top of LM-B (LM-Btop) is 56ms, suggesting a morphological uplift of 2 ms at the volcanic center area intersected by well T47.

4.3 Roof uplifting identified in seismic cube

There are three representative drilling wells, TZ-47, TZ-39 and TZ-35, with different distance to the uplift center (Fig. 2b). As shown in the seismic cross section (Fig. 6), drilling well T47 at the uplift center intersects the Xiaohaizi limestone (LM-X), which has markedly elevation and deformation. Several high amplitude bodies intersected by T47 are incased in the horizontal markers, including P-top (Permian-Triassic boundary), basalt-top (B-top), LM-S and LM-Btop. According to the down-well physical logging and the synthetic seismograms, the high amplitude bodies are corresponding to 7 basaltic layers, which have thickness ranging from 1.5 m to 100.4 m (Fig. 7). The pre-eruption morphology informed from the shape of B-top suggests a roof uplifting above the sills at TZ47, which extends to a ~4km wide area (Fig 2b).

Preprints (www.preprints.org) | NOT PEER-REVIEWED | Posted: 1 December 2020 doi:10.20944/preprints202012.0011.v1

Drilling well TZ-39 is 2476 m to the northwest of TZ47 and is located at the margin of the uplifting area. The Permian sedimentary strata show little disturbance by the intrusion of the sills and are similar to the strata distal to uplifting center, such as well TZ35, a well 6692 m to the east of well TZ47 (Fig. 2b).

5 Discussion

5.1 Sill and basalt thickness estimated by seismic method

Well T39 and well T47 are close enough but they have significant differences in velocity structure. The Paleozoic strata in the TZ35 column is very similar to that of TZ39 (Fig. 7); while TZ35 is 6692 m away from the enter (Fig.2b). This great distance can guarantee that the uplifting center had no structural or thermal influence on the TZ35 area. Therefore, the similarity between T39 and T35 indicate no remarkable deformation occur at these two wells. Wireline data also show that well T39 did not intersect with any intrusions (Fig. 7), thus the column of T39 can represent the stratigraphy prior to the deformation induced by the emplacement of magma at the T47 uplifting center.

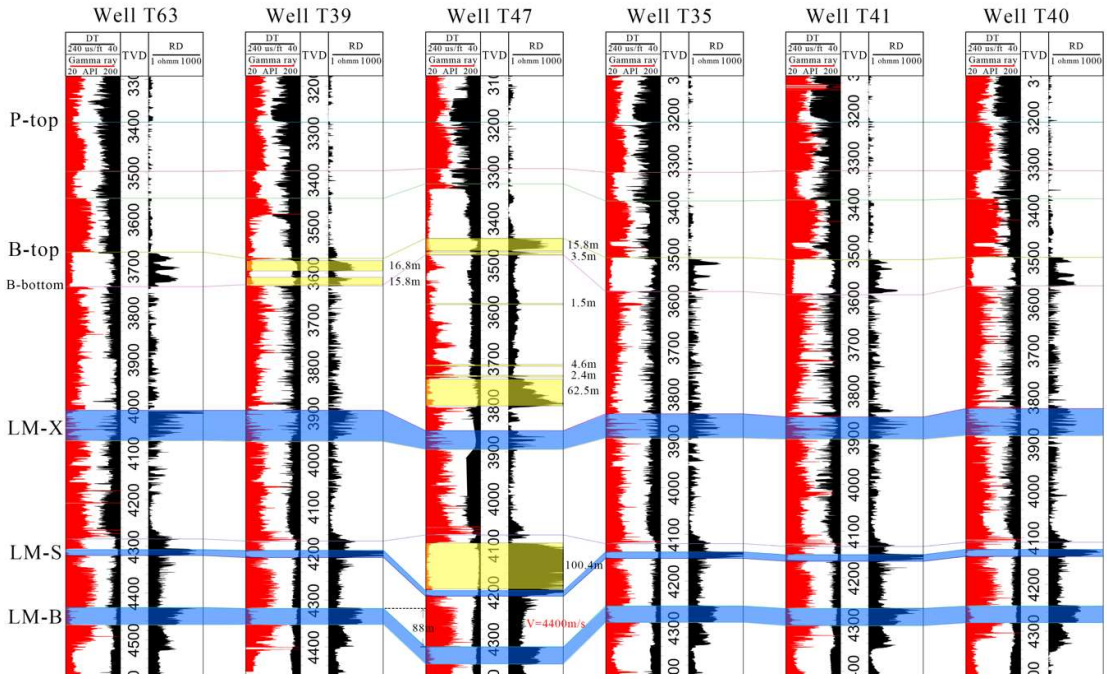

Fig. 7 Log profile flattened along the PT boundary (P-top). Yellow color stands for volcanic rocks. Blue color stands for limestones, which are Xiaohaizi limestones (LM-X), Standard limestones (LM-S) and bioclastic limestones (LM-B), respectively. The top of bioclastic limestones (LM-B) is abbreviated as LM-Btop in the text.

As shown in Fig. 4a, the thickness of host rock before emplacement of the sills is very stable. Therefore, the net difference between the top and bottom horizontal markers at each location after uplift should reflect the addition of basaltic sills, i.e., a magma intrusion-induced forced fold. However, the reflector of surface basalt lava flow at T47 is not so clear. We thus choose a higher reflector, the Permian-Triassic boundary (P-top), as the upper reference reflector to calculate the total

Preprints (www.preprints.org) | NOT PEER-REVIEWED | Posted: 1 December 2020 doi:10.20944/preprints202012.0011.v1

thickness of high velocity basalts, including sills and surface lava flows. The net difference between T39 and T47 can be calculated and correlated to the time depth section (Fig. 6) as described below:

(1) Select Permian-Triassic boundary (P-top) as top and bioclast limestone top surface (LM-Btop) as bottom. LM-Btop is beneath all seven volcanic layers at the location of T47, and is not affected by the igneous intrusions, thus this layer is used as a reference horizontal surface.

(2) The time difference between T39 and T47 at P-top ($\Delta t_{p\text{-}top}$) is 58 ms, and the time difference $\Delta t_{LM\text{-}Btop}$ at LM-Btop is 56 ms (Fig. 6). Comparing T39 and T47, the time thickness difference $\Delta t=\Delta t_{p\text{-}top}-\Delta t_{LM\text{-}Btop}=58-56=2$ ms.

(3) Flattening the well logging curves of T39 and T47 along the P-top, which represents a horizontal topography at the eruption time of the Permian flood basalt. The depth difference at LM-Btop between T39 and T47 can be calculated based on the logging data, which is $\Delta h=88$ m.

(4) According to the acoustic logging data (DT), the averaged acoustic velocity of T47 at the lowest 88 m (shown as Δh in Fig. 7) is $V_2=4450$ m/s; the dual time difference corresponding to the depth of difference is $\Delta t_l=\Delta h V_2\times2\times1000= 88/4450\times2\times1000=40$ ms.

(5) Likewise, by using the acoustic logging curve (DT), we can obtain the average velocity between P-top and LM-Btop from the two different lithologies: the average velocity of clastic rock is $V_{low}=3500$ m/s, the average velocity of volcanic rock is $V_{high}=5800$ m/s.

(6) The difference of pull-up time depth Δt_{VPU} due to igneous intrusions is equal to the time thickness difference between the two wells (obtained in step 2) minus the dual time difference corresponding to the depth of difference (obtained in step 4), i.e, $\Delta t_{VPU}= \Delta t_l -\Delta t =2-40=-38$ ms. The negative number here represents the direction of the time difference, at the velocity pull-up (VPU) case, Δt_{VPU} is negative.

(7) Following the VPU relationship proposed by Jackson [20], we can calculate the total thickness of basalt (H) by using:

$$H = \frac{\Delta t_{vpu} V_{low} V_{high}}{V_{high} - V_{low}} \quad (1)$$

H here represents the seismic recovered thickness of the high-velocity basaltic layers; V_{high}, V_{low}, and Δt_{VPU} are defined and obtained in steps 5 and 6.

By using $V_{high}=5800$ m/s, $V_{low}=3500$ m/s and $\Delta t_{VPU}=38$ms, the seismically recovered total thickness of the basaltic layers intersected by well T47 (H) is 167.7 m, and the total sill thickness (H_{sill}) at well T47 can be obtained by subtracting the thickness of surface lava flows, which is 167.7-15.8-3.5=148.4m.

5.2 Forced fold amplitude measured by wireline data

Down-slope flowing of lava may influence the thickness of basalt piles [36]. This means basalt flows at the outer rim of the forced fold may experience extra accumulation of magma while that at the central top of the forced fold may accumulate less thickness. Therefore, we use the bottom of the earliest basalt lava flow to represent the surface topography before basalt eruption. This can eliminate the effect of down slope magma flowing. Based on the logging data shown in Fig. 7, we can calculate the forced fold amplitude (A) by measuring the thickness difference between well T39 and well T47

Preprints (www.preprints.org) | NOT PEER-REVIEWED | Posted: 1 December 2020 doi:10.20944/preprints202012.0011.v1

immediately after the forced folding. This is calculated by comparing the distances from basalt bottom to the bottom of LM-S at T39 and T47. Depth of basalt bottom (B-bottom) is 2572m at T-39 and is 2402m at T47; depth of standard limestone bottom (LM-S) is 3151m at T-39 and is 3136m at T47. The forced fold amplitude (A) is (3136-2402) - (3151-2572) = 155m.

5.3 Discrepancy between fold amplitude and sill thickness

If we assume that forced folding of the overlain strata accommodates the intruded magma volume, the roof uplift amplitude should equal to the thickness of the intrusion [2]. However, there is a discrepancy that the fold amplitude (A=155m) is greater than the total sill thickness (H_{sill}=148.4m) at well T47, which is not expected in an elastic model. As for this type of discrepancy, Reeves et al. [11] gave three explanations: (i) the sills have a faster average interval velocity, which would increase the tuning limit of thin sills; (ii) the seismic velocity of the sedimentary sequence is overestimated, meaning that depth-converted fold amplitudes are accentuated; and/or (iii) multiple, seismically undetectable sills contributed to fold generation. However, in our case the sills can be detected directly by drilling wells and the velocities of sills and sediments can be well constrained by direct measurement of down-well logging data. We thus proposed another model to explain the discrepancy between A and H_{sill}. It is well-known that the molten magma has density lower than that of solidified rock. In the case of basalt from T47, the density of basaltic sills is 3.0 g/cm^3 and the molten magma with the same composition is 2.7 g/cm^3 [37]. During solidification, the 10% decrease of volume equals 3.5% decrease at one dimension. Therefore, the thickness of the intrusion when it was in the form of molten magma can be calculated by 148.4 / (1-3.5%) =153.8m, which is only 1.2 m difference from the seismic estimated up-roofing amplitude (A=155 m). This calculation suggests that the forced folding during intrusion of the sills was likely pure elastic. The decrease of total sill thickness during solidification may be compensated by uncompacting of the roof sediments, thus the original fold amplitude can be preserved.

5.4 The possible source of error in seismic study of forced fold

Most forced folding analyses are limited by the separability and detectability of seismic method, which is about ten meters and several tens of meters, respectively [11,38]. This means an error of up to several tens of meters when estimating folding amplitude. A more accurate way to constrain the fold amplitude and sill thickness is using drilling well data. In this study, the sills were intersected by several drilling wells and the lithologies are recorded by physical logging data. The concordant results of A and H_{sill} indicate that the space-making mechanism was elastic deformation. As shown in Fig. 7, three out of five sills have thickness ranging from 1.5 to 4.6 m, which are below the separability at main frequency of ~25 Hz and velocity range of 4000–7500 m/s for igneous intrusions [38]. In the seismic cross sections (Fig. 3 and Fig. S1), these sills are undetectable, and the folding amplitude (A) would be greater than the total thickness of sills (H_{sill}). This is demonstrated by a schematic cartoon shown in Fig. 8a. When a thin sedimentary stratum is interbedded with two sills (Fig. 8b), the seismic reflector may also be invisible if the thin sedimentary bed is below the resolving power. In this case the total thickness of the sills is overestimated due to the invisibility of interbedded sedimentary layer in the seismic cube.

Preprints (www.preprints.org) | NOT PEER-REVIEWED | Posted: 1 December 2020 doi:10.20944/preprints202012.0011.v1

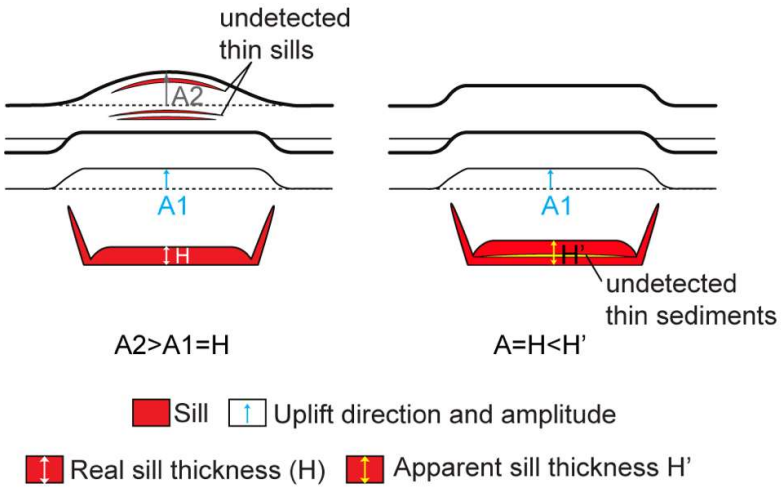

Fig. 8 Models showing how the ratio of fold amplitude (A) and sill thickness (H_{sill}) is overestimated or underestimated. (a) Schematic showing how the occurrence of seismically undetected, thin sills within the fold could produce the observed upward increase in fold amplitude, and the observed A2/H would be >1, which is larger than the real A/H_{sill}; (b) Schematic showing how the occurrence of seismically undetected, thin sedimentary layers within sills lead to overestimation of sill thickness, and the observed A/H' would be <1, which is smaller than the real A/H_{sill}.

In summary, when we study inelastic deformation component in a sill-induced forced folding process, the accuracy of fold amplitude and sill thickness is highly depended on separability and detectability of seismic method [11, 38]. Large uncertainties may occur if there are plenty of interbedded thin sills or thin sedimentary layers. Wireline data may be a better choice in measuring these parameters.

5 Conclusion

By interpretation of 3-D seismic data and down well logging data from the TZ-47 field, we find out that:

(1) Roof uplift is generated dominantly by elastic deformation induced by intrusion of the magma body in the TZ47 exploration area;

(2) When simply using seismic method, we may miss some invisible sills and interbedded sedimentary strata, which may result in underestimation or overestimation of sill thickness, respectively.

Supplementary Materials: The following are available online at www.mdpi.com/xxx/s1, Figure S1: Seismic profile showing the increasing tuning of basalt reflector. The bottom reflector (blue one) of the basalt layer from the center of the study area is not tuned; while that from the high thickness area are tuned, which means the thickness of basalt here has reached the tuning limit. Wells T40 and T41, which have basalt thickness of 72 m and 76 m, show tuning effect; while wells T39 and T35, which have basalt thickness of 52 m and 62m, show no tuning effect. This suggests that the tuning point should be slightly lower than 70 m, which is concordant with a tuning point at 25 Hz main frequency and a velocity of basalt at 5800 m/s.

Author Contributions: Conceptualization, Wei Tian; methodology, Lei Wang and Xiaomin Li; validation, Wei Tian; formal analysis, Xiaomin Li; investigation, Xiaomin Li; resources, Wei Tian and Lei Wang.; data curation, Lei Wang; writing—original draft preparation, Wei Tian; writing—review and editing, Wei Tian and Xiaomin Li; visualization, Xiaomin Li; supervision, Wei Tian; project administration, Wei Tian; funding acquisition, Wei Tian. All authors have read and agreed to the published version of the manuscript.

Funding: This research was funded by NSFC to WT, grant no. 41630205.

Acknowledgments: Dr. C. Magee is acknowledged for his thorough and thoughtful review on a former version of this manuscript. The Tarim Oil Field Company (TOFC), PetroChina Co. Ltd, is acknowledged for kindly providing seismic and wireline data for this research.

Conflicts of Interest: The authors declare no conflict of interest. The funders had no role in the design of the study; in the collection, analyses, or interpretation of data; in the writing of the manuscript, or in the decision to publish the results.

References

1. Cruden, A.R. On the emplacement of tabular granites. *J. Geol. Soc.* **1998**, *155*, 853-862, doi:DOI 10.1144/gsjgs.155.5.0853.
2. Hansen, D.M.; Cartwright, J. Saucer-shaped sill with lobate morphology revealed by 3D seismic data: implications for resolving a shallow-level sill emplacement mechanism. *J. Geol. Soc.* **2006**, *163*, 509-523, doi:10.1144/0016-764905-073.
3. Magee, C.; Hunt Stewart, E.; Jackson, C.A.L. Volcano growth mechanisms and the role of sub-volcanic intrusions: Insights from 2D seismic reflection data. *Earth and Planetary Science Letters* **2013**, *373*, 41-53, doi:10.1016/j.epsl.2013.04.041.
4. Magee, C.; Jackson, C.A.L.; Hardman, J.P.; Reeve, M.T. Decoding sill emplacement and forced fold growth in the Exmouth Sub-basin, offshore northwest Australia: Implications for hydrocarbon exploration. *Interpretation* **2017**, *5*, SK11-SK22, doi:10.1190/int-2016-0133.1.
5. Johnson, A.M.; Pollard, D.D. Mechanics of growth of some laccolithic intrusions in henry mountains, utah .1. Field observations, gilberts model, physical properties and flow of magma. *Tectonophysics* **1973**, *18*, 261-309, doi:10.1016/0040-1951(73)90050-4.
6. Pollard, D.D.; Johnson, A.M. Mechanics of growth of some laccolithic intrusions in henry mountains, utah .2. Bending and failure of overburden layers and sill formation. *Tectonophysics* **1973**, *18*, 311-354, doi:10.1016/0040-1951(73)90051-6.
7. Stearns, D.W.; Matthews, V., III. Faulting and forced folding in the Rocky Mountains foreland. In *Laramide Folding Associated with Basement Block Faulting in the Western United States*, Geological Society of America: 1978; Vol. 151, p. 0.
8. Sturkell, E.; Einarsson, P.; Sigmundsson, F.; Geirsson, H.; Olafsson, H.; Pedersen, R.; de Zeeuw-van Dalfsen, E.; Linde, A.T.; Sacks, S.I.; Stefansson, R. Volcano, geodesy and magma dynamics in Iceland. *Journal of Volcanology and Geothermal Research* **2006**, *150*, 14-34, doi:10.1016/j.jvolgeores.2005.07.010.
9. Sparks, R.S.J.; Biggs, J.; Neuberg, J.W. Monitoring Volcanoes. *Science* **2012**, *335*, 1310-1311, doi:10.1126/science.1219485.
10. Ebmeier, S.K.; Andrews, B.J.; Araya, M.C.; Arnold, D.W.D.; Biggs, J.; Cooper, C.; Cottrell, E.; Furtney, M.; Hickey, J.; Jay, J., et al. Synthesis of global satellite observations of magmatic and volcanic deformation: implications for volcano monitoring & the lateral extent of magmatic domains. *Journal of Applied Volcanology* **2018**, *7*, 2, doi:10.1186/s13617-018-0071-3.
11. Reeves, J.; Magee, C.; Jackson, C. Unravelling intrusion-induced forced fold kinematics and ground

deformation using 3D seismic reflection data. *Volcanica* **2018**, 1-17.

12. Magee, C.; Hoggett, M.; Jackson, C.A.L.; Jones, S.M. Burial-Related Compaction Modifies Intrusion-Induced Forced Folds: Implications for Reconciling Roof Uplift Mechanisms Using Seismic Reflection Data. *Front Earth Sc-Switz* **2019**, *7*, doi:UNSP 3710.3389/feart.2019.00037.
13. Morgan, S.; Stanik, A.; Horsman, E.; Tikoff, B.; de Saint Blanquat, M.D.; Habert, G. Emplacement of multiple magma sheets and wall rock deformation: Trachyte Mesa intrusion, Henry Mountains, Utah. *Journal of Structural Geology* **2008**, *30*, 491-512, doi:10.1016/j.jsg.2008.01.005.
14. Schmiedel, T.; Kjoberg, S.; Planke, S.; Magee, C.; Galland, O.; Schofield, N.; Jackson, C.A.L.; Jerram, D.A. Mechanisms of overburden deformation associated with the emplacement of the Tulipan sill, mid-Norwegian margin. *Interpretation* **2017**, *5*, SK23-SK38, doi:10.1190/int-2016-0155.1.
15. Schmiedel, T.; Galland, O.; Haug, O.T.; Dumazer, G.; Breitkreuz, C. Coulomb failure of Earth's brittle crust controls growth, emplacement and shapes of igneous sills, saucer-shaped sills and laccoliths. *Earth and Planetary Science Letters* **2019**, *510*, 161-172, doi:10.1016/j.epsl.2019.01.011.
16. Schofield, N.J.; Brown, D.J.; Magee, C.; Stevenson, C.T. Sill morphology and comparison of brittle and non-brittle emplacement mechanisms. *J. Geol. Soc.* **2012**, *169*, 127-141, doi:10.1144/0016-76492011-078.
17. Galland, O.; Spacapan, J.B.; Rabbel, O.; Maira, K.; Soto, F.G.; Eiken, T.; Schiuma, M.; Leanza, H.A. Structure, emplacement mechanism and magma-flow significance of igneous fingers - Implications for sill emplacement in sedimentary basins. *Journal of Structural Geology* **2019**, *124*, 120-135, doi:10.1016/j.jsg.2019.04.013.
18. Spacapan, J.B.; Galland, O.; Leanza, H.A.; Planke, S. Igneous sill and finger emplacement mechanism in shale-dominated formations: a field study at Cuesta del Chihuido, Neuquen Basin, Argentina. *J. Geol. Soc.* **2017**, *174*, 422-433, doi:10.1144/jgs2016-056.
19. Hansen, D.M.; Cartwright, J. The three-dimensional geometry and growth of forced folds above saucer-shaped igneous sills. *Journal of Structural Geology* **2006**, *28*, 1520-1535, doi:10.1016/j.jsg.2006.04.004.
20. Jackson, C.A.L.; Schofield, N.; Golenkov, B. Geometry and controls on the development of igneous sill-related forced folds: A 2-D seismic reflection case study from offshore southern Australia. *Geological Society of America Bulletin* **2013**, *125*, 1874-1890, doi:10.1130/b30833.1.
21. Magee, C.; Bastow, I.D.; de Vries, B.V.; Jackson, C.A.L.; Hetherington, R.; Hagos, M.; Hoggett, M. Structure and dynamics of surface uplift induced by incremental sill emplacement. *Geology* **2017**, *45*, 431-434, doi:10.1130/g38839.1.
22. Zhang, S.b.; Ni, Y.N.; Gong, F.H.; Lu, H.N.; Huang, Z.B.; Lin, H.L. *A Guide to the Stratigraphic Investigation on the Periphery of the Tarim Basin*; Beijing, 2003; pp. 1-280.
23. Lu, S.; Li, H.; Zhang, C.; Niu, G. Geological and geochronological evidence for the Precambrian evolution of the Tarim Craton and surrounding continental fragments. *Precambrian Research* **2008**, *160*, 94-107, doi:https://doi.org/10.1016/j.precamres.2007.04.025.
24. Li, Z.X.; Li, X.H.; Kinny, P.D.; Wang, J.; Zhang, S.; Zhou, H. Geochronology of Neoproterozoic syn-rift magmatism in the Yangtze Craton, South China and correlations with other continents: evidence for a mantle superplume that broke up Rodinia. *Precambrian Research* **2003**, *122*, 85-109, doi:https://doi.org/10.1016/S0301-9268(02)00208-5.
25. Yang, S.; Chen, H.; Li, Z.; Li, Y.; Yu, X.; Li, D.; Meng, L. Early Permian Tarim Large Igneous Province in northwest China. *Science China Earth Sciences* **2013**, *56*, 2015-2026, doi:10.1007/s11430-013-4653-y.
26. Tian, W.; Campbell, I.H.; Allen, C.M.; Guan, P.; Pan, W.; Chen, M.; Yu, H.; Zhu, W. The Tarim picrite-basalt-rhyolite suite, a Permian flood basalt from northwest China with contrasting rhyolites

produced by fractional crystallization and anatexis. *Contributions to Mineralogy and Petrology* **2010**, *160*, 407-425, doi:10.1007/s00410-009-0485-3.

27. Yang, J.; Zhu, W.; Guan, D.; Zhu, B.; Yuan, L.; Xiang, X.; Su, J.; He, J.; Wu, X. 3D seismic interpretation of subsurface eruptive centers in a Permian large igneous province, Tazhong Uplift, central Tarim Basin, NW China. *International Journal of Earth Sciences* **2016**, *105*, 2311-2326.
28. Xu, Y.-G.m.; Wei, X.; Luo, Z.-Y.; Liu, H.-Q.; Cao, J. The Early Permian Tarim Large Igneous Province: Main characteristics and a plume incubation model. *Lithos* **2014**, *204*, 20-35, doi:10.1016/j.lithos.2014.02.015.
29. Wang, L.; Tian, W.; Shi, Y.; Guan, P. Volcanic structure of the Tarim flood basalt revealed through 3-D seismological imaging. *Sci. Bull.* **2015**, *60*, 1448-1456, doi:10.1007/s11434-015-0866-0.
30. Smallwood, J.R.; Maresh, J. The properties, morphology and distribution of igneous sills: modelling, borehole data and 3D seismic from the Faroe-Shetland area. *Geological Society London Special Publications* **2002**, *197*, 271-306.
31. Posamentier, H.W. Application of 3D seismic visualization techniques for seismic stratigraphy, seismic geomorphology and depositional systems analysis: examples from fluvial to deep-marine depositional environments. *Geological Society, London, Petroleum Geology Conference series* **2005**, *6*, 1565-1576, doi:10.1144/0061565.
32. Schofield, N.; Heaton, L.; Holford, S.P.; Archer, S.G.; Jackson, C.A.L.; Jolley, D.W. Seismic imaging of 'broken bridges': linking seismic to outcrop-scale investigations of intrusive magma lobes. *J. Geol. Soc.* **2012**, *169*, 421-426, doi:10.1144/0016-76492011-150.
33. Thomson, K.; Hutton, D. Geometry and growth of sill complexes: insights using 3D seismic from the North Rockall Trough. *Bulletin of Volcanology* **2004**, *66*, 364-375, doi:10.1007/s00445-003-0320-z.
34. Wang, L.; Tian, W.; Shi, Y. Data Processing Methods for 3D Seismic Imaging of Subsurface Volcanoes: Applications to the Tarim Flood Basalt. *Journal of visualized experiments: JoVE* **2017**, e55930, doi:10.3791/55930 (2017).
35. Li, D.X.; Yang, S.F.; Chen, H.L.; Cheng, X.G.; Li, K.; Jin, X.L.; Li, Z.L.; Li, Y.Q.; Zou, S.Y. Late Carboniferous crustal uplift of the Tarim plate and its constraints on the evolution of the Early Permian Tarim Large Igneous Province. *Lithos* **2014**, *204*, 36-46, doi:10.1016/j.lithos.2014.05.023.
36. Dragoni, M.; Bonafede, M.; Boschi, E. Downslope Flow Models of a Bingham Liquid - Implications for Lava Flows. *Journal of Volcanology and Geothermal Research* **1986**, *30*, 305-325, doi:Doi 10.1016/0377-0273(86)90059-4.
37. Wang, L.; Tian, W.; Wei, Z.H.; Gong, M.Y.; Li, X.M. Volcanic conduits of the Tarim Flood Basalt Province: 3D structure and thermogenic gas release. *Acta Petrol. Sin.* **2018**, *34*, 75-90.
38. Magee, C.; Maharaj, S.M.; Wrona, T.; Jackson, C.A.L. Controls on the expression of igneous intrusions in seismic reflection data. *Geosphere* **2015**, *11*, 1024-1041, doi:10.1130/ges01150.1.

Supplementary Fig. S1

Preprints (www.preprints.org) | NOT PEER-REVIEWED | Posted: 1 December 2020 doi:10.20944/preprints202012.0011.v1

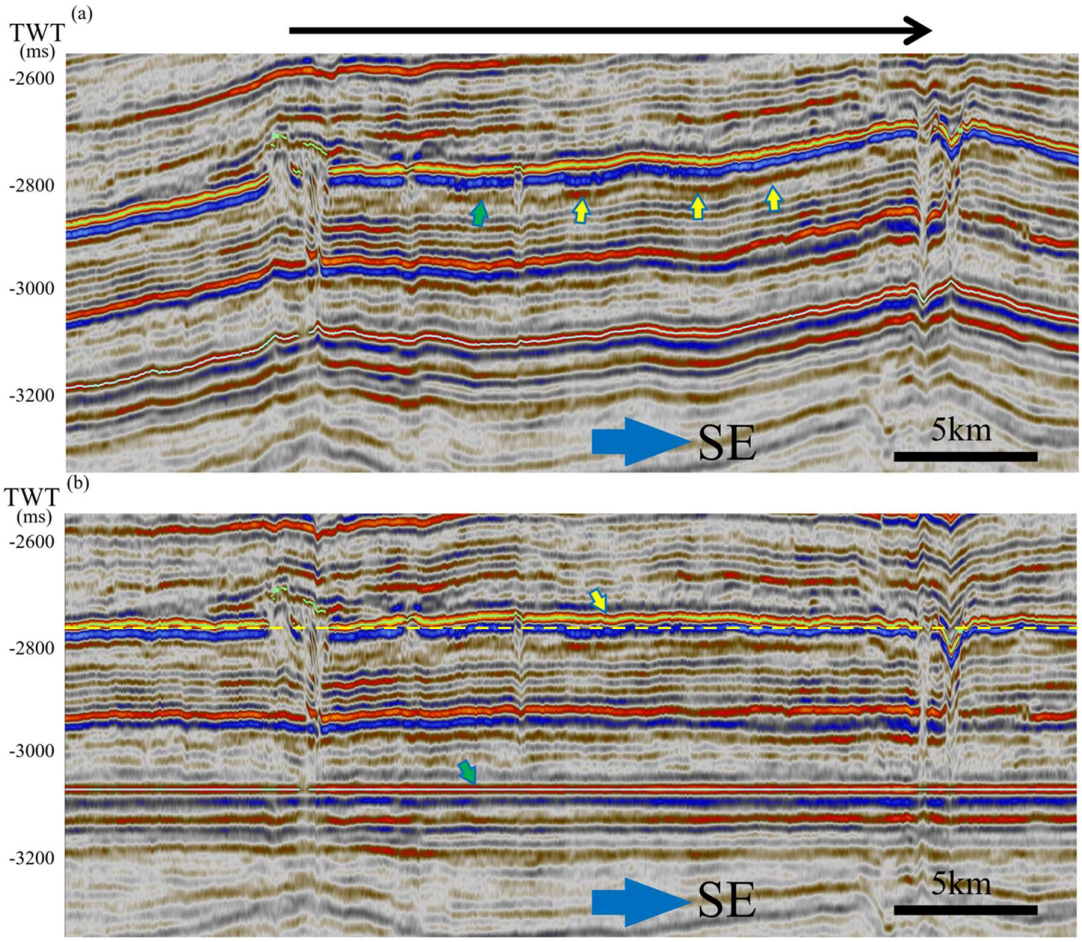

Figure S1: Seismic profile showing the increasing tuning of basalt reflector. The bottom reflector (blue one) of the basalt layer from the center of the study area is not tuned; while that from the high thickness area are tuned, which means the thickness of basalt here has reached the tuning limit. Wells T40 and T41, which have basalt thickness of 72 m and 76 m, show tuning effect; while wells T39 and T35, which have basalt thickness of 52 m and 62m, show no tuning effect. This suggests that the tuning point should be slightly lower than 70 m, which is concordant with a tuning point at 25 Hz main frequency and a velocity of basalt at 5800 m/s.